Anomalous Hall Effect from Frustration-Tuned Scalar Chirality Distribution in $Pr_2Ir_2O_7$

M. Udagawa[1,2] and R. Moessner[2]

[1]Department of Applied Physics, University of Tokyo, Tokyo 113-8656, Japan
[2]Max-Planck-Institut für Physik komplexer Systeme, 01187 Dresden, Germany

(Received 25 July 2012; published 17 July 2013)

We study the anomalous Hall effect due to noncoplanar magnetism on a pyrochlore structure. We focus on the frustration-induced spatial inhomogeneity of different magnetic low-temperature regimes, between which one can efficiently tune using an external magnetic field. We incorporate nonmagnetic scattering on a phenomenological level so that we can distinguish between the effects of short-range correlations and short-range coherence. We obtain a Hall conductivity (σ_H) as a function of field strength and direction which compares well to the experimental data of $Pr_2Ir_2O_7$. In particular, we show that the observed peak in σ_H for $\mathbf{H} \parallel [111]$ signals the crossover from zero-field spin ice to kagome ice.

DOI: 10.1103/PhysRevLett.111.036602 PACS numbers: 72.10.−d, 71.10.Fd, 71.23.−k, 71.27.+a

The properties of itinerant degrees of freedom on geometrically frustrated lattices are only poorly understood. One promising avenue for studying the interplay of frustration and itinerance is hybrid systems where itinerant electrons interact with localized magnetic moments subject to strong frustration. The latter can exhibit various exotic phases, incorporating peculiar spatial correlations [1]. It is therefore natural to ask whether these bequeath their unusual behavior to the itinerant electrons, resulting in novel types of behavior for the composite system.

The anomalous Hall effect (AHE) is one particularly striking resulting phenomenon [2]. The AHE was originally associated with ferromagnetic conductors with strong spin-orbit interaction [3–5]. However, the AHE has recently been reinterpreted in a broader context, including noncoplanar magnets as promising candidates for its emergence [6–9].

Prominently, the compound $Pr_2Ir_2O_7$ shows a unique Hall response. It is composed of two interpenetrating pyrochlore lattices. Ir $5d$ electrons form a conduction band on one, while the localized Pr $4f$ moments reside on the other and develop spin-ice-type correlation at low temperature [10,11]. It is quite plausible that the spin scalar chirality of the spin-ice manifold gives rise to nontrivial features in the Hall response, particularly strikingly in zero field [12]. In addition, the observed Hall conductivity is highly anisotropic and nonmonotonic, with a prominent peak around $H \sim 0.7$ T for $\mathbf{H} \parallel [111]$ [9,12,13]. Pioneering analyses of the pyrochlore conductors [14,15] have considered spatially periodic structures for the localized moments. It is now natural to ask how spatial aperiodicity—arising from the geometrical frustration of the spin-ice local moments—manifests itself in the nontrivial Hall response observed in this compound.

For this purpose, we adopt a model in which itinerant electrons interact with $\langle 111\rangle$-type localized Ising moments on a pyrochlore lattice. To clarify the relation between the Hall response and spin-ice correlations, we assume the Ising moments to obey the nearest-neighbor spin-ice model, rather than the RKKY interaction mediated by electrons [16]. This phenomenological model turns out to describe the experimental data of $Pr_2Ir_2O_7$ quite well. In particular, we find that the prominent peak observed for $\mathbf{H} \parallel [111]$ can be attributed to the crossover from the zero-field spin-ice state to kagome ice: the latter is a state with perfectly field-aligned spins on the triangular layer with the other spins disordered but subject to the ice rule constraint [17]; see the Supplemental Material [18].

In the remainder of this work, we first define and analyze a simple kagome-ice conduction model, which allows systematic understanding of the Hall conductivity of spatially inhomogeneous systems. In particular, we can establish the validity of third-order perturbation theory for the weak-coupling region. This is then built into the phenomenological model to make detailed contact with the $Pr_2Ir_2O_7$ data.

The kagome-ice conduction model is defined as itinerant electrons under the local fields $\mathbf{h}_i$ at each site of the kagome lattice [Figs. 1(a) and 1(b)], where $\{\mathbf{h}_i\}$ are imposed by the localized Ising moments $\{\mathbf{S}_i\}$ obeying the kagome-ice rule as introduced below. The Hamiltonian is given by

$$\mathcal{H} = -t \sum_{\langle i,i'\rangle,\alpha} (c^{\dagger}_{i\alpha} c_{i'\alpha} + \mathrm{H.c.}) - \sum_{i,\alpha,\beta} c^{\dagger}_{i\alpha} \boldsymbol{\sigma}_{\alpha\beta} c_{i\beta} \cdot \mathbf{h}_i. \tag{1}$$

The sum $\langle i, i'\rangle$ is taken over the nearest-neighbor sites. We simply choose $\mathbf{h}_i = J\mathbf{S}_i$, with exchange coupling J. The localized spins $\{\mathbf{S}_i\}$ are subject to local easy-axis anisotropy, i.e., $\mathbf{S}_i = \eta_i \mathbf{D}_i$ $(\eta_i = \pm 1)$, with $\mathbf{D}_i = (1/\sqrt{3})[1, -1, 1]$, $(1/\sqrt{3})[1, 1, -1]$, and $(1/\sqrt{3})[-1, 1, 1]$, if i belongs to sublattices A, B, and C. Here, we take a quenched average in terms of $\{\mathbf{S}_i\}$ by imposing the "kagome-ice rule"; namely, we impose for each triangle $\sum_{i\in\triangle} \eta_i = 1$.

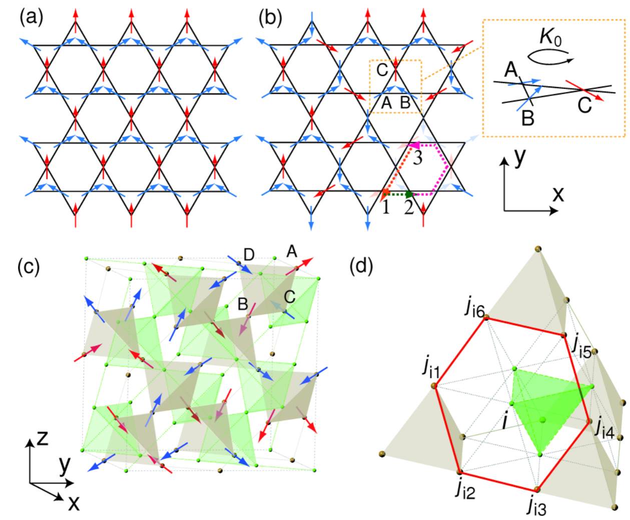

FIG. 1 (color online). (a) A uniform configuration and (b) a representative of the disordered configurations satisfying the kagome-ice rule. Blue (red) arrows show spins $\mathbf{S}_i$ corresponding to $\eta_i = 1(-1)$. An example of the graph belonging to $G[7]$ (see the main text) is shown in (b) with three combined dashed arrows. (c) Structure of double-pyrochlore lattice. Tetrahedra with (without) arrows constitute Pr (Ir) pyrochlore lattice. Sublattice indices A, B, C, and D are shown for the Pr lattice, for which an example of a spin-ice configuration is shown. (d) One Ir tetrahedron surrounded by four Pr tetrahedra. Each Ir ion (i) has six neighboring Pr ions ($j_{i1}, \ldots, j_{i6}$) forming a hexagon, as highlighted by a thick line.

This allows a macroscopic number of spin configurations [19,20], including a uniform configuration [Fig. 1(a)], and a huge number of disordered configurations [Fig. 1(b)]. Crucially, for each and all of these, the spin scalar chirality is uniform $\mathbf{S}_a \cdot (\mathbf{S}_b \times \mathbf{S}_c) = K_0 \equiv -4/3\sqrt{3}$ for all the upward and downward triangles [21]. We can thus examine the effect of spatial disorder on the AHE, while preserving uniform spin scalar chirality.

For the calculation of Hall conductivity σ_{xy}, we randomly generate a series of spin configurations under the kagome-ice rule $\{\mathbf{S}_i^{(p)}\}$. For each $\{\mathbf{S}_i^{(p)}\}$, the Hall conductivity is given as

$$\sigma_{xy}(\{\mathbf{S}_i^{(p)}\}) = \frac{e^2}{\hbar V} \sum_{m,m'} [f(E_m) - f(E_{m'})] \times \frac{\mathrm{Im}(\langle m|J_x|m'\rangle\langle m'|J_y|m\rangle)}{(E_m - E_{m'})^2 + 1/\tau^2}, \qquad (2)$$

by the Kubo formula [22]. Here, $|m\rangle$ and E_m are the eigenenergy and corresponding eigenstate of Hamiltonian Eq. (1). $f(E)$ is the Fermi distribution function at zero temperature. $J_{x(y)}$ is the $x(y)$ component of the current operator, and V is the total volume of the system. Here, we introduce the phenomenological damping rate $1/\tau$ to take account of the finite lifetime of electrons due to nonmagnetic impurities. While the magnetic disorder itself causes damping, nonmagnetic scattering plays another important role in Hall conductivity. $1/\tau$ sets a coherence length of electrons, which determines the effective spatial scale of spin scalar chirality. The Hall conductivity σ_{xy} can be obtained after taking the configurational average, as $\sigma_{xy} = (1/N_s)\sum_{p=1}^{N_s} \sigma_{xy}(\{\mathbf{S}_i^{(p)}\})$. We typically choose $N_s = 100$ and system size $N = 32 \times 32 \times 3 = 3072$ sites. Hereafter, we set $t = \hbar = e^2/h = 1$.

In Figs. 2(a) and 2(b), we show the dependence of σ_{xy} on particle density n in the uniform [Fig. 1(a)] and disordered configurations [Fig. 1(b)], at $1/\tau = 1.0$. In the uniform case, σ_{xy} shows a steep change around $n \sim 1/3$ due to the singularity in Berry curvature: At $J = 0$, the band structure is described by a tight-binding model on a kagome lattice, which has Dirac cones at 1/3 filling.

The J and $1/\tau$ dependence of σ_{xy} is summarized in Fig. 2(c) at $n = 0.0977$. First, for small J, a cubic law $\sigma_{xy} \propto J^3$ is found in both uniform and disordered cases. This cubic law can perturbatively be ascribed to the multiple scattering from triplets of spins exhibiting finite scalar chirality [23]. With increasing J, deviation from the cubic law is found at $J \sim 1/\tau$. In particular, in the uniform case, σ_{xy} becomes insensitive to $1/\tau$, and another scaling law $\sigma_{xy} \propto J$ appears, suggesting the σ_{xy} is described in terms of the Berry curvature in this region [24]. For $J \gg t$, the system falls into a double-exchange regime: the itinerant electron spins are aligned with the localized spins, and σ_{xy} takes on values only weakly dependent on $1/\tau$.

In general, σ_{xy} takes considerably different values between the disordered case (σ_{xy}^d) and the uniform ordered one σ_{xy}^u, as shown in Fig. 2(d), where we plot the $1/\tau$ dependence of σ_{xy} at $J = 0.05$. This is most pronounced for small damping $1/\tau \ll J$, where σ_{xy}^u saturates, but the difference persists all the way to $1/\tau \gg J$.

A perturbative treatment in $\mathbf{h}$ sheds light on the origin of difference between the two cases. To third order [25],

$$\sigma_{xy} = \sum_{(i_1,i_2,i_3)} \mathbf{h}_{i_1} \cdot (\mathbf{h}_{i_2} \times \mathbf{h}_{i_3}) W_{xy}(i_1, i_2, i_3), \qquad (3)$$

where the summation is taken over the $N(N-1) \times (N-2)/6$ triplets of sites (i_1, i_2, i_3); see the Supplemental Material [18]. This gives the Hall conductivity as summation over the triplets' spin scalar chirality with weighting factor $W_{xy}(i_1, i_2, i_3)$. It is instructive to resolve the Hall conductivity (3) in the form of a graphical series expansion as $\sigma_{xy} = \sum_{m=3}^{\infty} \sigma_{xy}^{(m)}$. Here, $\sigma_{xy}^{(m)}$ is the total contribution from the triplets (i_1, i_2, i_3) belonging to the set of graphs $G[m]$ composed of three segments of total length m. [An example of a triplet $\in G[7]$ is shown in Fig. 1(b).]

Figures 2(e) and 2(f) show the partial summation $S_{xy}^{(m)} \equiv \sum_{l=3}^{m} \sigma_{xy}^{(l)}$ and the averaged weighting factor at each m, $W_{xy}^{(m)}$, at $J = 0.1$ and $1/\tau = 0.5$. In the disordered case,

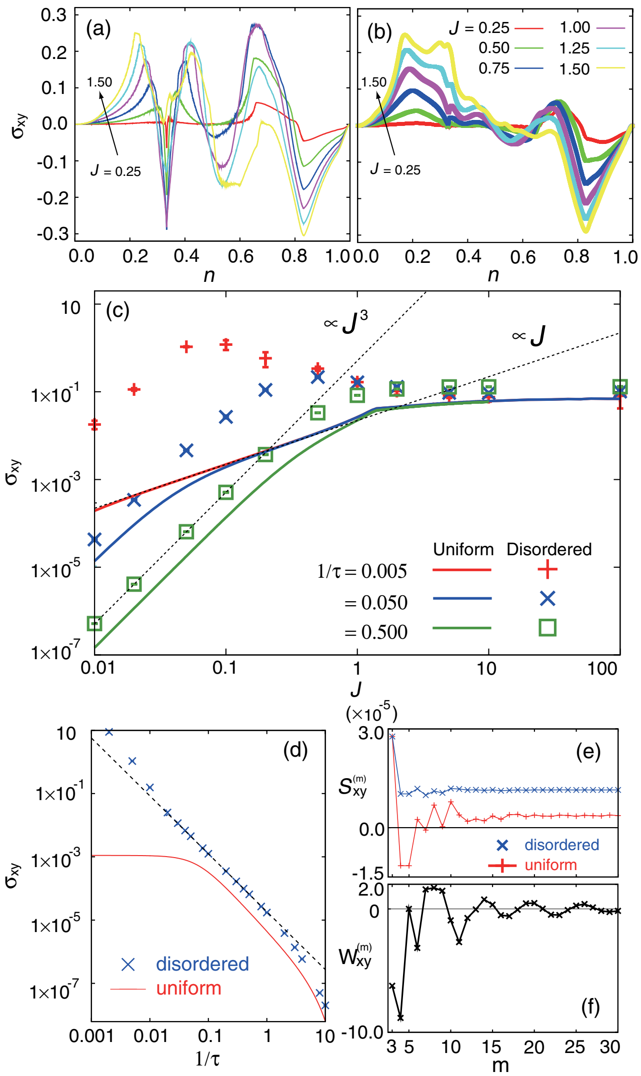

FIG. 2 (color online). Dependence of σ_{xy} on particle density n for (a) the uniform configuration and (b) the disordered configuration at $1/\tau = 1.00$. (c) J dependence of σ_{xy} at $n = 0.0977$ for the disordered case (dots) and the uniform case (solid lines): $1/\tau = 0.005$, 0.050, and 0.500 from top to bottom. (d) The $1/\tau$ dependence of σ_{xy} at $n = 0.0977$ and $J = 0.05$. The dashed line is a guide to eye. (e) Partial summation of Hall conductivity $S_{xy}^{(m)}$. (f) The weighting factor $W_{xy}^{(m)}$ averaged over the graphs at each m.

different contributions for graphs of a given $m \geq 5$ come with an effectively random sign, hence canceling against one another. By contrast, for the uniform case, the summation continues to oscillate until damping destroys coherence at larger m. This illustrates the different roles played by loss of correlations of the local moments and loss of coherence of the itinerant electrons in the two respective cases.

Keeping in mind the insights obtained from the kagome-ice conduction model, let us turn to $Pr_2Ir_2O_7$. We consider a double-pyrochlore lattice: two interpenetrating pyrochlore lattices, as shown in Fig. 1(c), with itinerant electrons ($c_{i\alpha}$) on the Ir sublattice and localized Pr moments ($\{\mathbf{S}[j]\}$) on the other. The localized moments are subject to Ising anisotropy as $\mathbf{S}[j] \equiv \eta_j \mathbf{D}_j$, with $\mathbf{D}_j = (1/\sqrt{3})[1, 1, 1]$, $(1/\sqrt{3})[1, -1, -1]$, $(1/\sqrt{3})[-1, 1, -1]$, and $(1/\sqrt{3})[-1, -1, 1]$, if j belongs to sublattices A, B, C, and D, respectively. Each site i on the Ir sublattice has six neighbors ($j_{i1}, j_{i2}, \ldots, j_{i6}$) located on the honeycomb ring of the Pr sublattice, as shown in Fig. 1(d). To describe the interaction, we adopt the Hamiltonian Eq. (1), with the local field given by the sum of the six neighboring localized moments $\mathbf{h}_i = J\sum_{l=1}^{6}\mathbf{S}[j_{il}]$. We apply the third-order perturbative scheme to this model. Since the exchange coupling J stems from the superexchange process between Pr and Ir ions, it is reasonable to assume that $J/t \ll 1$.

To connect the Hall conductivity and observed spin-ice correlation in $Pr_2Ir_2O_7$, we phenomenologically assume that the moments $\mathbf{S}[j]$ obey the nearest-neighbor spin-ice Hamiltonian Eq. (4), rather than determine them by solving Eq. (1) self-consistently:

$$\mathcal{H}_{\text{spin}} = J_{\text{spin}} \sum_{\langle j,j' \rangle} \eta_j \eta_{j'} - \mathbf{H} \cdot \sum_j \mathbf{S}[j] \quad (J_{\text{spin}} > 0). \quad (4)$$

We use $\mathcal{H}_{\text{spin}}$ in a standard equilibrium Monte Carlo sampling to obtain $N_s = 100$ sets of $\{\mathbf{S}[j]\}$ and input them into Eq. (1) through $\mathbf{h}_i$. Although we are interested in the region $T \to 0$, we introduce temperature T as a phenomenological parameter to mimic the deviation from ideal spin ice due to the long-range RKKY interaction in the actual compound and set $T/J_{\text{spin}} = 0.5$.

Hereafter, we focus on the field directions $\mathbf{H} \parallel [100]$ and [111] [26]. We set magnetic coordinates $\mathbf{e}_x \parallel [010]$ and $\mathbf{e}_y \parallel [001]$ for $\mathbf{H} \parallel [100]$, and $\mathbf{e}_x \parallel [\bar{1}10]$ and $\mathbf{e}_y \parallel [\bar{1}\,\bar{1}\,2]$ for $\mathbf{H} \parallel [111]$, and calculate $\sigma_H \equiv \sigma_{xy}$. We consider the low density region [9] and fix the particle density at $n = 0.01$. As a system size, we adopt $N = 12 \times 12 \times 12 \times 4 = 6912$ sites.

In Figs. 3(a) and 3(b), we plot the magnetic field dependence of σ_H at $1/\tau = 5.0$ and 0.5. For extremely large damping $1/\tau = 5.0$, only the smallest triangles contribute to σ_H [Fig. 3(d)]. In this region, the sign of σ_H becomes opposite between $\mathbf{H} \parallel [100]$ and $\mathbf{H} \parallel [111]$, as expected in Ref. [9] on the assumption of the local limit. However, the full magnetic field dependence of σ_H, especially the low-field negative linear response in this local limit considerably deviates from the experimental results [9] [Fig. 3(a), inset]. The negative linear response comes from the large negative contribution at $m = 3$ [Fig. 3(d)]: solely short-range spin-ice correlations within the four-Pr cluster [Fig. 1(d)] do not give correct σ_H.

In contrast, for intermediate damping $1/\tau = 0.5$, σ_H shows quite similar behavior to the experimental data [9]. For small H, σ_H shows positive linear response irrespective of the field direction [Fig. 3(b), inset]. In Fig. 3(e), we plot the graph-resolved Hall conductivity at $H = 0.4$ for $\mathbf{H} \parallel [111]$. This plot shows that the spatially extended

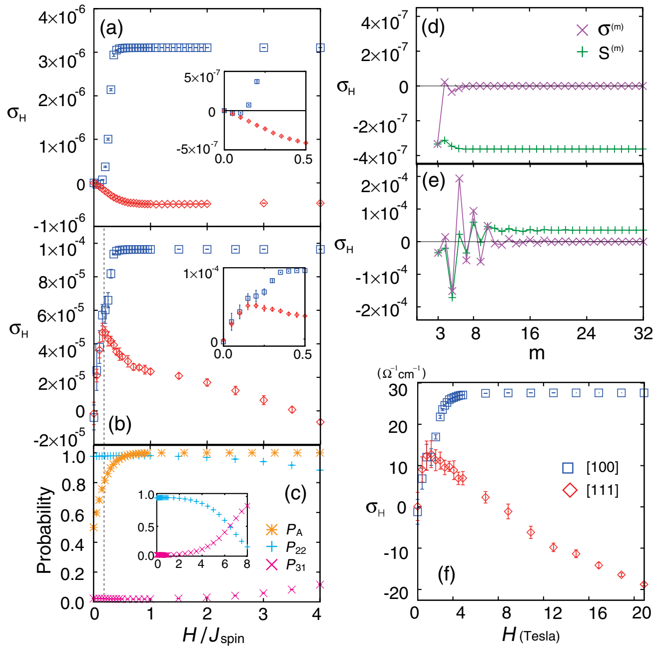

FIG. 3 (color online). The magnetic field (H) dependence of σ_H at $n = 0.01$ and $J = 0.1$ for $\mathbf{H} \parallel [100]$ and [111] at (a) $1/\tau = 5.0$ and (b) 0.5. The results for $\mathbf{H} \parallel [100]$ ([111]) are plotted with open squares (diamonds). The insets are enlarged plots around $H = 0$. (c) H dependence of the probabilities P_{22}, P_{31}, and P_A. The crossing of P_{22} and P_{31} is shown in the inset. The vertical dashed line in (b) and (c) is a guide to eye. (d), (e) Graph-resolved Hall conductivity $\sigma_H^{(m)}$ and its partial summation $S_H^{(m)}$ at $H/J_{\rm spin} = 0.4$ and $\mathbf{H} \parallel [111]$ for (d) $1/\tau = 5.0$ and (e) 0.5. (f) σ_H of the multiorbital model.

scalar chirality beyond the local limit ($m \lesssim 10$, or roughly 35 Å) plays a crucial role in the positive linear response.

The low-field peak for $\mathbf{H} \parallel [111]$ is the most conspicuous feature of the Hall conductivity in $Pr_2Ir_2O_7$. In previous studies [9,15], this peak is attributed to the spin flip crossover from the low-field spin-ice state with a dominant two-in-two-out configuration to the high-field saturated state with three-in-one-out and one-in-three-out spin configurations. However, our analysis suggests a different picture. In Fig. 3(c), we plot the probabilities that each tetrahedron is occupied by two-in-two-out configuration (P_{22}), and three-in-one-out or one-in-three-out configurations (P_{31}). This plot shows that P_{22} and P_{31} are almost constant at low fields, until the spin flip crossover happens at much higher field $H \sim 6J_{\rm spin}$ [17] [Fig. 3(c), inset].

The peak of σ_H seems rather related to the crossover from the zero-field spin-ice state to the kagome-ice state. In Fig. 3(c), we plot the probability that a spin on the sublattice A aligns parallel to the field (P_A), as an indicator of the kagome-ice state. P_A changes from 0.5 at $H = 0$ to 1.0 at the kagome-ice state. The peak of σ_H corresponds to $P_A \sim 0.75$, i.e., the midpoint of this saturation process, clearly showing that the peak signals the crossover to a kagome-ice state. Within the nearest-neighbor spin-ice model used here, the crossover occurs at $H \sim T$. Accordingly, the peak is located at $H \sim 0.5T$; see the Supplemental Material [18]. Indeed, the [111] magnetization takes $\sim(1/3)M_{\rm sat}$ experimentally, when σ_H has a peak, with $M_{\rm sat} \sim 1.5\mu_B/\mathrm{Pr}$, the saturated magnetization [9]. This magnetization ($\sim(1/3)M_{\rm sat}$) coincides with the value at the midpoint of the saturation process of M_A, and smaller than $M_s \sim (5/6)M_{\rm sat}$ expected at the spin flip crossover.

Here, let us turn to the physical origin of the peak. As the magnetic field is applied, net spin scalar chirality, and hence σ_H, is enhanced. On the other hand, the evolution to the kagome-ice state can be regarded as a partial ordering process of sublattice A, so that spatial disorder is reduced, suppressing the interference between the graphs, resulting in a suppression of σ_H, as discussed above for the kagome-ice model. It is tempting to note that the balance between the two effects gives rise to a prominent peak during the evolution to the kagome-ice state. Indeed, the peak becomes more prominent as $1/\tau$ is further reduced (not shown), reinforcing the subtle balance between the two competing effects. The sensitivity to $1/\tau$ may be confirmed from the systematic study of the sample dependence of σ_H and resistivity. Further analyses are clearly desirable to elucidate this point.

We finally comment on the quantitative aspect of our theory. Although our result is based on a single-orbital tight-binding model, the overall features of σ_H are insensitive to band structure. However, the amplitude of the Hall conductivity is sensitive to the "details" of the band structure. By adopting a realistic band structure based on a multiorbital tight-binding model with three t_{2g} orbitals, we could obtain the Hall conductivity $\sim 30\ \Omega^{-1}\,\mathrm{cm}^{-1}$ at high fields, comparable to experimental data [Fig. 3(f)], with reproducing various features of experimental results; see the Supplemental Material [18].

The authors thank S. Nakatsuji, Y. Machida, and Y. Motome for fruitful discussions. This work was supported by KAKENHI (Grants No. 24740221, No. 23102708, and No. 24340076). The computation in this work has been partially done using the facilities of the Supercomputer Center, Institute for Solid State Physics, University of Tokyo.

Note added.—Related work has recently been done in Ref. [27], which focuses on an effective chirality coupling in $Pr_2Ir_2O_7$.

[1] For an overview, see R. Moessner and A. P. Ramirez, Phys. Today **59**, No. 2, 24 (2006).
[2] For a recent review, N. Nagaosa, J. Sinova, S. Onoda, A. H. MacDonald, and N. P. Ong, Rev. Mod. Phys. **82**, 1539 (2010).
[3] R. Karplus and J. M. Luttinger, Phys. Rev. **95**, 1154 (1954).

[4] J. Smit, Physica (Amsterdam) **21**, 877 (1955).
[5] L. Berger, Phys. Rev. B **2**, 4559 (1970).
[6] K. Ohgushi, S. Murakami, and N. Nagaosa, Phys. Rev. B **62**, R6065 (2000).
[7] M. Taillefumier, B. Canals, C. Lacroix, V. K. Dugaev, and P. Bruno, Phys. Rev. B **74**, 085105 (2006).
[8] Y. Taguchi, Y. Oohara, H. Yoshizawa, N. Nagaosa, and Y. Tokura, Science **291**, 2573 (2001).
[9] Y. Machida, S. Nakatsuji, Y. Maeno, T. Tayama, T. Sakakibara, and S. Onoda, Phys. Rev. Lett. **98**, 057203 (2007).
[10] S. Nakatsuji, Y. Machida, Y. Maeno, T. Tayama, T. Sakakibara, J. Duijn, L. Balicas, J. Millican, R. Macaluso, and J. Chan, Phys. Rev. Lett. **96**, 087204 (2006).
[11] M. Udagawa, H. Ishizuka, and Y. Motome, Phys. Rev. Lett. **108**, 066406 (2012).
[12] Y. Machida, S. Nakatsuji, S. Onoda, T. Tayama, and T. Sakakibara, Nature (London) **463**, 210 (2009).
[13] L. Balicas, S. Nakatsuji, Y. Machida, and S. Onoda, Phys. Rev. Lett. **106**, 217204 (2011).
[14] A. Kalitsov, B. Canals, and C. Lacroix, J. Phys. Conf. Ser. **145**, 012020 (2009).
[15] T. Tomizawa and H. Kontani, Phys. Rev. B **82**, 104412 (2010).
[16] In previous studies, conduction electrons and localized moments were treated self-consistently in a Monte Carlo framework [Y. Motome and N. Furukawa, Phys. Rev. Lett. **104**, 106407 (2010)] or by cluster dynamical mean-field theory [11]. However, these methods are not available in the current setting, since accurate determination of the dc Hall conductivity requires system sizes that are currently unattainable.
[17] Z. Hiroi, K. Matsuhira, S. Takagi, T. Tayama, and T. Sakakibara, J. Phys. Soc. Jpn. **72**, 411 (2003).
[18] See Suppelemental Material at http://link.aps.org/supplemental/10.1103/PhysRevLett.111.036602 for the crossover between spin ice and kagome ice, details of the third-order perturbation theory, and comparison with experiments.
[19] M. Udagawa, M. Ogata, and Z. Hiroi, J. Phys. Soc. Jpn. **71**, 2365 (2002).
[20] R. Moessner and S. L. Sondhi, Phys. Rev. B **68**, 064411 (2003).
[21] Here the sites a, b, and c are chosen in a counterclockwise fashion.
[22] R. Kubo, J. Phys. Soc. Jpn. **12**, 570 (1957).
[23] G. Tatara and H. Kawamura, J. Phys. Soc. Jpn. **71**, 2613 (2002).
[24] M. Onoda, G. Tatara, and N. Nagaosa, J. Phys. Soc. Jpn. **73**, 2624 (2004).
[25] σ_{xy} in this perturbative scheme does not precisely correspond to the Hall conductivity obtained from the numerical diagonalization method, due to the different treatment of the damping parameter $1/\tau$.
[26] Here, we do not consider $\mathbf{H} \parallel [110]$, which requires detailed microscopic knowledge beyond the nearest-neighbor spin-ice model. See, e.g., M. Gingras, in *Introduction to Frustrated Magnetism*, edited by C. Lacroix, P. Mendels, and F. Mila (Springer-Verlag, Berlin, 2011), p. 293.
[27] R. Flint and T. Senthil, Phys. Rev. B **87**, 125147 (2013).